ISSN 1064-2269, Journal of Communications Technology and Electronics, 2017, Vol. 62, No. 9, pp. 927–940. © Pleiades Publishing, Inc., 2017.
Original Russian Text © S.E. Bankov, E.V. Frolova, 2017, published in Radiotekhnika i Elektronika, 2017, Vol. 62, No. 9, pp. 833–846.

ELECTRODYNAMICS AND WAVE PROPAGATION

Synthesis and Analysis of a Planar Waveguide Array with Two-Dimensional Frequency Scanning Focused in the Fresnel Zone

S. E. Bankov* and E. V. Frolova

Kotel'nikov Institute of Radio Engineering and Electronics, Russian Academy of Sciences, Moscow, 125009 Russia
**e-mail: sbankov@yandex.ru*

Received May 27, 2016

Abstract—A 2D array of radiators with raster frequency scanning focused in the Fresnel zone is presented. The problem of determining the radiator positions for field focusing at a finite distance from the array plane is solved. An approximate matrix model of the array antenna describing its properties as a microwave multiport and allowing determination of the distribution of radiation sources in the array aperture is proposed. The problem of improvement of the array matching in scanning ranges is considered. An approximate model describing radiation from the array is built. This model is used for determining the position and shape of the scanning surface and the field distribution inside the focal spot as well as for the analysis of the dynamics of the field maximum in the frequency scanning sector.

DOI: 10.1134/S1064226917090030

INTRODUCTION

At present, active and passive short-range radio imaging systems are widely used for examination, mine search, and medical diagnosing. An important part of such systems is a scanning or a multibeam radio lens, which forms images. There are many publications devoted to the development and analysis of radio lenses [1–10].

Radio lenses used in such systems are antennas of different types focused in the Fresnel zone: antennas with mechanical scanning, phased array antennas (PAAs), as well as multibeam reflector and lens systems and antenna arrays. Radio lenses with electrical scanning and multibeam lenses, which can form the image in real time, are of the greatest interest. Since radio imaging systems usually operate at relatively high frequencies (from the upper part of the centimeter wave band to the terahertz band) and realization of high angular resolution requires a rather large aperture, the cost of a lens with a 2D PAA is too high. In practice, radio lenses with hybrid type of scanning, mechanical in one plane and electrical in the other plane, are commonly used.

The hybrid operating mode can be most simply implemented on the basis of frequency scanning with the use of a leaky-wave antenna [11]. In this case, the space surveillance in the other plane may be either mechanical or electrical with the use of analog phase shifters, digital phasing, or a multibeam quasi-optical system [12, 13]. Such a design of the radio lens can substantially decrease the number of controlled elements and, as a consequence, the cost of this lens without lowering the angular and range resolutions. Note that improvement of economic parameters is attained at the cost of the loss in multifunctionality and flexibility typical of the PAA lenses.

Radiation can be focused in the Fresnel zone with the use of various types of leaky-wave antennas: antennas based on a curvilinear waveguide [14, 15]; a rectilinear irregular waveguide with varying phase velocity of the leaky mode [16, 17]; rectilinear waveguides with varying period of radiating irregularities [18, 20]; spiral waveguides [21]; and a radial line [22, 23]. Note that the frequency scanning mode was analyzed only in [16, 17] for the case of a linear leaky-wave array with constant period.

A 2D array of weakly directional radiators with varying period focused in the Fresnel zone at a distance on the order of the array aperture is considered in [24]. Frequency scanning characteristic are analyzed by the example of a planar slotted-guide array of parallel rectangular metal waveguides. Radio lenses based on such arrays scan the space by combining two scanning methods. In one plane, which is parallel to the waveguides forming the array, the focal spot is moved by means of frequency scanning. In the other plane, which is orthogonal to the waveguide axes, the space can be scanned with the use of different methods: with the help of a linear PAA or a multibeam beam-forming network. In any case, surveillance is reduced to formation of a set of waves exciting the

array channels with a given amplitude–phase distribution. Here, the main factor needed for scanning is the phase distribution of the wave amplitudes.

Let us call the aforementioned scanning planes the parallel and perpendicular planes. As in the parallel plane, the focal plane can be moved in the perpendicular plane with the help of frequency scanning. Arrays with 2D or raster frequency scanning radiating into the far zone are known for a very long time (see, e.g., [25]).

This type of scanning is ensured with the use of special devices (scanners). A scanner is a transmission line connected to waveguides forming an array. Sections of the scanner's transmission line connecting adjacent waveguides have lengths exceeding the spacing between the waveguides. Due to this fact, the rate of change of the phase distribution of the waves exciting the waveguides is many times higher than the rate of change of the phase distribution inside the waveguides of the array. For this reason, the main beam of the array pattern moves rather slowly along the parallel plane and rapidly along the perpendicular plane. Motion in the perpendicular plane is periodically repeated as frequency varies, because the array radiates on the Floquet harmonics with different numbers.

It should be noted that a scanner is a rather bulky device substantially increasing overall dimensions and weight of the antenna. The design of an array with 2D frequency scanning that does not require a scanner is described in [26]. Radiating waveguides of the array are connected with the use of connecting waveguides introduced in the design and playing the role of a scanner. These waveguides taken together form an integrated zigzag transmission line (ZTL) with included radiating elements. The main advantages of an antenna based on an array with raster frequency scanning are its simple design and low cost due to the absence of a large number of controlled elements as in a PAA or transmitting–receiving modules as in a multibeam array.

This study is devoted to the analysis of an array with raster frequency scanning on the basis of a ZTL focused in the Fresnel zone. In this paper, we solve the following problems:

(i) Determination of the radiator coordinates and the length of radiating and connecting waveguides that ensure field focusing at a specified focal point.

(ii) Building of a matrix array model that allows calculation of the wave amplitudes inside the ZTL and determination of the sources exciting the array radiators.

(iii) Analysis of the array as a microwave multiport; determination of the frequency scanning ranges; selection of the waveguide parameters ensuring matching of the array at center frequencies of the scanning ranges.

(iv) Building of a model describing the array radiation field.

(v) Analysis of the array scanning characteristics, including determination of the surface along which the field maximum moves with varying frequency and obtaining the frequency dependence of the maximum amplitude.

1. STRUCTURE OF THE ARRAY AND SYNTHESIS OF ITS PARAMETERS

The structure under study is schematically shown in Fig. 1. It consists of N radiating and connecting waveguides, which can generally have different propagation constants γ_r and γ_c, respectively. The spacing between waveguides along the $0x$ axis is designated by P_x. The waveguide axes are located at the following points x_n:

$$x_n = nP_x - \frac{D_x}{2}, \quad n = 0,\ldots,N-1, \qquad D_x = (N-1)P_x. \tag{1}$$

The radiators are placed along the $0y$ axis at points with coordinates $y_{n,m}$, $m = 0,\ldots,M-1$, which will be determined below.

The waveguides can be conventionally separated into two parts: the part with constant length D_y along the $0y$ axis and the part with variable length dL_n. We assume that each radiating waveguide contains the same number of radiators and its part with constant length contains all radiators. Waveguide sections with variable length are required for formation of a nonlinear phase distribution of the amplitudes of exiting waves at the inputs of radiating waveguides. We assume that the inputs of radiating waveguides are located in the lower part of the structure and the working input of the entire structure has number *1* (see Fig. 1). The radiating and connecting waveguides are connected by turners T, which represent microwave two-ports with scattering matrix $\hat{S}_t$.

The array focuses the field at the point with coordinates $0, 0, z_f$, as shown in Fig. 2. Conditions of exact focusing are fulfilled at center frequency f_0. Let us choose distance D_y from the following condition:

$$(\gamma_{c0} + \gamma_{r0})D_y = 2\pi\nu_0, \tag{2}$$

where $\gamma_{r,c0}$ are the waveguide propagation constants at frequency f_0 and ν_0 is an integer number. Note that, strictly speaking, when determining the propagation constant of a radiating waveguide, it is necessary to take into account the phase shift specified by the radiators. If all radiators are identical and each radiator shifts the wave phase by $\Delta\varphi_r$, effective propagation

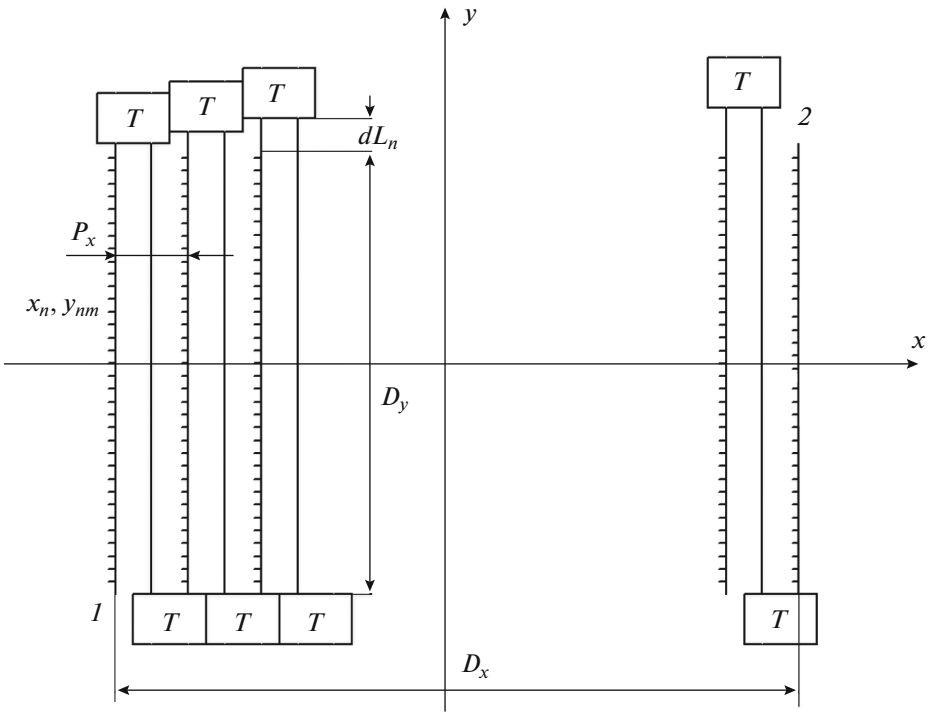

Fig. 1. Block diagram of an array with raster frequency scanning.

constant of the radiating waveguide γ_{re} can be written as follows:

$$\gamma_{re} = \gamma_r - \frac{M\Delta\varphi_r}{D_y}, \tag{3}$$

where γ_r is the propagation constant of a waveguide without radiators. Note that we take the following time dependence of the fields: $\exp(i\omega t)$. As a result, the propagating wave accumulates a negative phase.

However, the addition to constant γ_r is very small and consideration for this addition does not introduce fundamental changes in the description of this array. In this study, we perform our analysis under the assumption of $\Delta\varphi_r = 0$. Thus, we assume that γ_{r0} in relationship (2) is the propagation constant of an unperturbed waveguide.

Note that, without sections with lengths dL_n, condition (2) ensures equiphase excitation of all radiating waveguides at frequency f_0. Hence, using these sections, it is possible to create a special phase distribution φ_n of waves in the array channels.

It can be readily seen that phase distribution φ_n is related (to within inessential term $2\pi\nu_0$) to lengths dL_n by the relationship

$$\varphi_n = -(\gamma_{c0} + \gamma_{r0})\sum_{p=1}^{n} dL_{p-1}, \quad n = 1,\ldots N-1, \qquad \varphi_0 = 0. \tag{4}$$

Using formula (4), we can readily obtain the expression for lengths dL_n:

$$dL_n = -\frac{\varphi_{n+1} - \varphi_n}{\gamma_{c0} + \gamma_{r0}}. \tag{5}$$

The condition of focusing at focal point F is reduced to the condition of equal optical lengths trav-

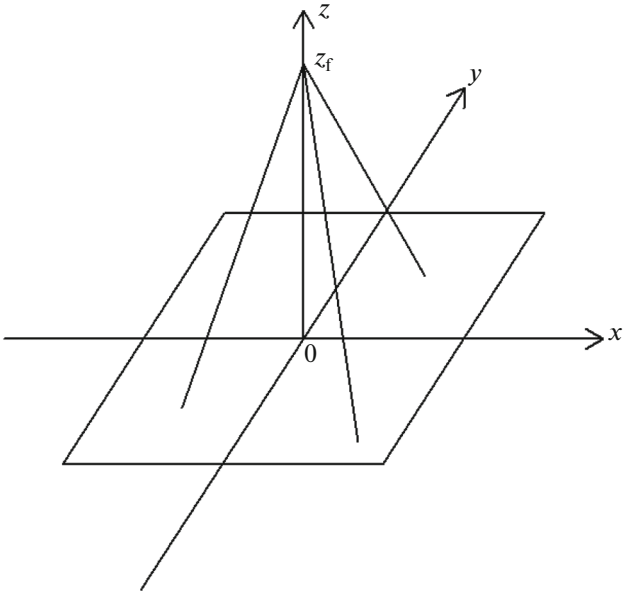

Fig. 2. Field focusing by the array.

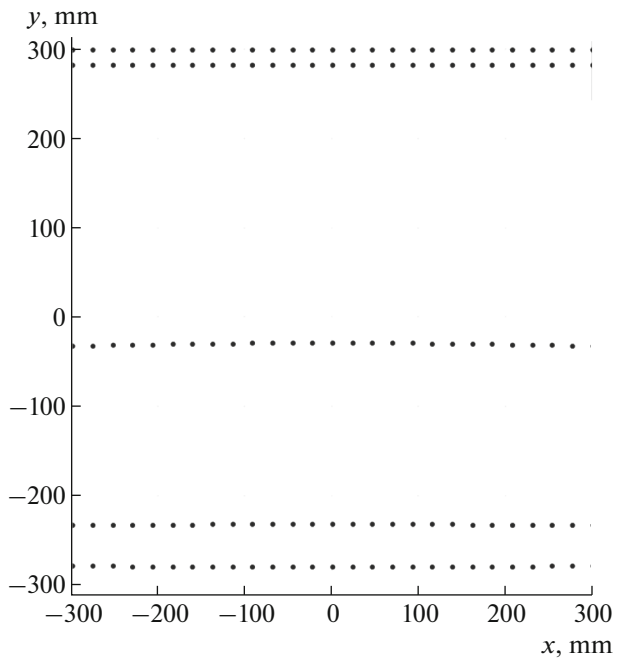

Fig. 3. Positions of radiators in the array plane.

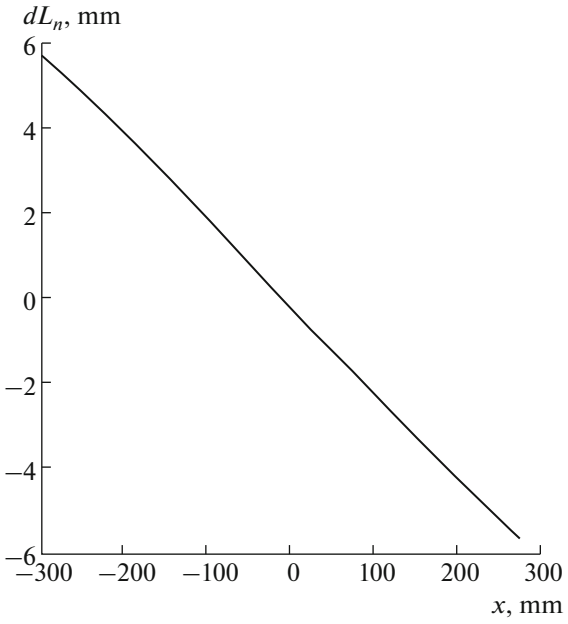

Fig. 4. Dependence of length dL_n on coordinate x.

eled by the waves from the inputs of radiating waveguides to the focus:

$$\begin{aligned} &-\gamma_{r0}(y_{n,m} - D_y/2) + \varphi_n \\ &- k_0\sqrt{y_{n,m}^2 + x_n^2 + z_f^2} = 2\pi m, \end{aligned} \tag{6}$$

where m is an integer number and k_0 is the wave number of free space at synthesis frequency f_0. Relationship (6) is written under the assumption of equiphase radiation of all array radiators in the case of equiphase excitation of these radiators by waveguide modes. In practice, there are arrays in which radiators can be excited with an additional phase shift of π. Among such arrays are the well-known slotted-guide arrays in which the phase of the radiated wave can be shifted by π by shifting the slots in opposite directions from the center of the broad wall. Focusing condition (6) is not changed for such an array, except for expression πm appearing on the right-hand side.

Note that focusing condition (6) is practically the same as the expression obtained in [24]. Omitting details of solution of Eq. (6) for unknowns $y_{n,m}$, we give here the final result:

$$\begin{aligned} y_{n,m} &= -\frac{U_{r0}P_{n,m}}{1-U_{r0}^2} + \sqrt{\left(\frac{U_{r0}P_{n,m}}{1-U_{r0}^2}\right)^2 - \left(x_n^2 + z_f^2 - P_{n,m}^2\right)}, \\ U_{r0} &= \frac{\gamma_{r0}}{k_0}, \quad P_{n,m} = \frac{\varphi_n - 2\pi m\varepsilon}{k_0} + U_{r0}\frac{D_y}{2}, \end{aligned} \tag{7}$$

where $\varepsilon = 1$ for an array with equiphase excitation and $\varepsilon = 0.5$ for an array with alternating-phase excitation.

Choosing initial phases φ_n, it is possible to optimize the distribution of radiators in the array aperture. This issue was considered in [24] where it has been shown that it is reasonable to choose the radiator positions with the use of an additional condition. For such a condition, it is convenient to choose field focusing in the initial section of the array at $y = -D_y/2$:

$$\varphi_n = k_0\sqrt{\left(\frac{D_y}{2}\right)^2 + x_n^2 + z_f^2}. \tag{8}$$

For such a choice of initial phases, the radiators are located near the nodes of a rectangular grid (Fig. 3), which is convenient from the viewpoint of design.

The dependence of length dL_n on coordinate x is shown in Fig. 4. This dependence was obtained for $D_y = 600$ and $z_f = 800$. Hereinafter, all dimensions are given in millimeters. It is seen that the distribution of waveguide lengths is asymmetric with respect to the point $x = 0$. In spite of this fact, the phase distribution is described by even function (8).

Note that the analysis of relationship (2) points to the zonal structure of the frequency scanning range, because condition (2) of equal phases of the waves exciting the radiating waveguides can be fulfilled not only for $\nu = \nu_0$. For $\nu \neq \nu_0$, it is fulfilled at frequencies f_ν. Here, $f_{\nu_0} = f_0$. Condition (2) ensures focusing in the plane $x = 0$. However, at frequencies f_ν different from the synthesis frequency, the focal spot will be shifted along coordinate y. Within some frequency interval near f_ν, the spot moves along a line that is almost parallel to axis $0x$. We will see below that, at a

large deviation from frequency f_ν, the field intensity in the spot experiences distortions limiting the scanning region within one zone. Therefore, the subsequent scanning process is associated with transition into another zone with another value of ν and another zone center frequency f_ν.

2. MATRIX MODEL OF THE ARRAY

The problem of the synthesis of the array parameters ensuring field focusing at frequency f_0 was solved in Section 1. We can now pass to building an array model in the form of a set of microwave multiports. Let us describe radiators with the help f scattering matrices $\hat{S}_\mathrm{r}$:

$$\hat{S}_\mathrm{r} = \begin{bmatrix} S_{\mathrm{r}11} & S_{\mathrm{r}12} \\ S_{\mathrm{r}12} & S_{\mathrm{r}11} \end{bmatrix}, \quad S_{\mathrm{r}11} = -\frac{y}{2+y}, \qquad (9)$$
$$S_{\mathrm{r}12} = 1 + S_{\mathrm{r}11}.$$

Scattering matrix $\hat{S}_\mathrm{r}$ is written under the assumption of symmetric and reciprocal radiators. Expressions for elements of the scattering matrix correspond to the equivalent circuit of a radiator in the form of admittance y, which is connected in parallel to the transmission line. Such a circuit is typical of a longitudinal slot in the broad waveguide wall.

Generally, admittance y is a complex frequency-dependent quantity. This dependence is close to the dependence of a parallel resonant circuit [26]. In this study, we do not consider the influence of the frequency dependence of the radiator characteristics on operation of the array and describe it by real-valued conductance g.

A factor important for building of a correct model of the array is consideration for the reflection from the turner, which is described by scattering matrix $\hat{S}_\mathrm{t}$:

$$\hat{S}_\mathrm{t} = \begin{bmatrix} iq & \sqrt{1-q^2} \\ \sqrt{1-q^2} & iq \end{bmatrix}. \qquad (10)$$

The scattering matrix of the turner is written with consideration for the reciprocity and unitarity conditions [27] of the two-port. In this case, its elements are completely specified by parameter q, which may depend on frequency.

The radiators and turners are connected by sections of transmission lines, which have scattering matrix $\hat{S}_\mathrm{l}$:

$$\hat{S}_\mathrm{l} = \begin{bmatrix} 0 & \exp(-i\gamma L) \\ \exp(-i\gamma L) & 0 \end{bmatrix}, \qquad (11)$$

where γ is the propagation constant of the transmission line and L is its length.

As seen from Fig. 1, the entire array can be considered as a cascade connection of the sections of transmission lines, radiators, and turners. Such a structure can be conveniently described with the use of wave transmission matrices $\hat{T}_{\mathrm{r,t,l}}$, which are related to the scattering matrix in a certain way [27].

Transmission matrix of the entire array $\hat{T}_\mathrm{a}$ is expressed through transmission matrices of the array components as follows:

$$\hat{T}_\mathrm{a} = \left(\prod_{n=0}^{N-2} \hat{T}_{\mathrm{sa},n} \right) \hat{T}_{\mathrm{sa},N-1}, \qquad (12)$$

where $\hat{T}_{\mathrm{sa},n}$ is the transmission matrix of a subarray, which consists of a radiating waveguide, a waveguide section with length dL_n, a turner, a one more waveguide section with length dL_n, a connecting waveguide, and a turner. The last subarray with number $N-1$ has a simpler structure in the form of one radiating waveguide.

Let us write the transmission matrix of a subarray as follows:

$$\hat{T}_{\mathrm{sa},n} = \left(\prod_{m=0}^{M-1} \hat{T}_{\mathrm{l},n,m} \hat{T}_r \right) \hat{T}_{dL,n} \hat{T}_\mathrm{t} \hat{T}_{dL,n} \hat{T}_\mathrm{cw} \hat{T}_\mathrm{t}, \qquad (13)$$

where $\hat{T}_{\mathrm{l},n,m}$ is the transmission matrix of the section of radiating waveguide connecting two adjacent radiators, $\hat{T}_{dL,n}$ is the transmission matrix of the waveguide section with length dL_n, and $\hat{T}_\mathrm{cw}$ is the transmission matrix of the connecting waveguide.

Transition from the transmission matrix to the scattering matrix is performed with the help of well-known relationships [27].

Let us first consider the frequency dependence of the elements of the scattering matrix of entire array $\hat{S}_\mathrm{a}$ in a wide frequency band. Frequency dependences of absolute values of the array reflection and transmission coefficients are shown in Figs. 5 and 6, respectively. The results were obtained for $g = 0.005$, $q = 0.15$, $f_0 = 9$ GHz, $P_x = 23$, $D_y = 600$, $z_f = 700$, and $\varphi_n = 0$. The transmission line, which is the basis of the array, is a hollow metal waveguide with the size of the broad wall $a = 22$. The radiating waveguide and the connecting (coupling) waveguide are chosen identical.

The frequency dependence of reflection and transmission coefficients contains a periodic sequence of maxima and minima. The maximum of the reflection coefficient takes substantial values ranging from 0.7 to 0.8. It is important that the reflection coefficient reaches the maximum value at synthesis frequency f_0 and all center frequencies of scanning zones f_ν. The array transmission coefficient rapidly decreases at the same frequencies.

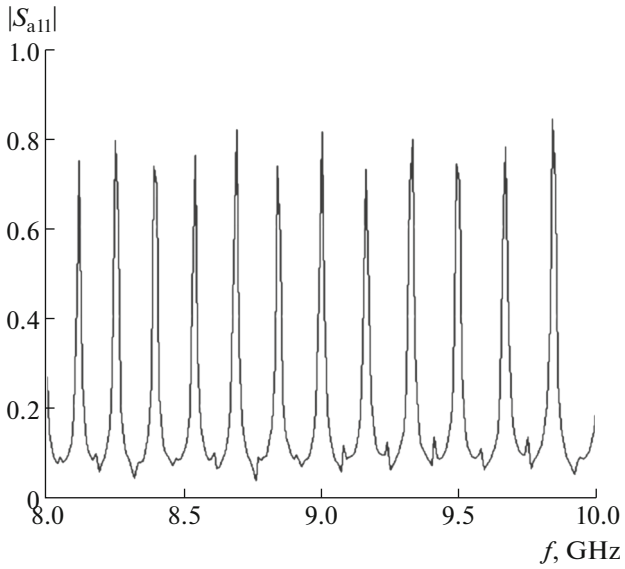

Fig. 5. Frequency dependence of the absolute value of the reflection coefficient at the array input for $\varphi_n = 0$.

The absolute value of the maximum reflection coefficient weakly depends on radiator conductance g and is almost completely specified by parameter q, i.e., the reflection coefficient of the transition. However, it should be noted that it does not decrease in proportion to q. As this parameter decreases, the burst of the reflection coefficient becomes narrower but its maximum value still remains rather large.

Curves in Figs. 5 and 6 were obtained under the condition $\varphi_n = 0$, which enables simple explanation of the appearance of sharp bursts of the reflection coefficient. These bursts are caused by the effect of summation of a large number of waves with small amplitudes reflected from the turners. They are summed in phase at frequencies f_v. Since the array is a periodic structure at $\varphi_n = 0$, we can speak of formation of forbidden zones of this array in the vicinities of frequencies f_v.

We can suppose that introduction of phase shifts φ_n should improve matching of this structure, since, in this case, the lengths of waveguides become different, the structure is no longer periodic, and the effect of equiphase summation of waves becomes weaker. The frequency dependence of the absolute value of the reflection coefficient obtained for the parameters given above and values of φ_n chosen with the help of relationship (8) is shown in Fig. 7. It is seen that introduction of phase shifts does not result in a fundamental improvement of the array matching. Maximum reflection levels decrease only slightly and the maximum is slightly shifted from frequency f_0, which improves matching at the synthesis frequency and at frequencies f_v. However, this shift is insufficiently large to ensure satisfactory operation of the array for scanning in a frequency band.

The problem of matching can be substantially mitigated by using radiating and connecting waveguides with different propagation constants. For example, we can use a waveguide partially filled with a dielectric with relative permittivity ε as a connecting (coupling) waveguide. In this case, in the course of synthesis, we can impose additional conditions equivalent to (2):

$$\gamma_{c0} D_y = 2\pi(N_0 + 1/2), \quad \gamma_{r0} D_y = 2\pi(N_0 - 1/2). \quad (14)$$

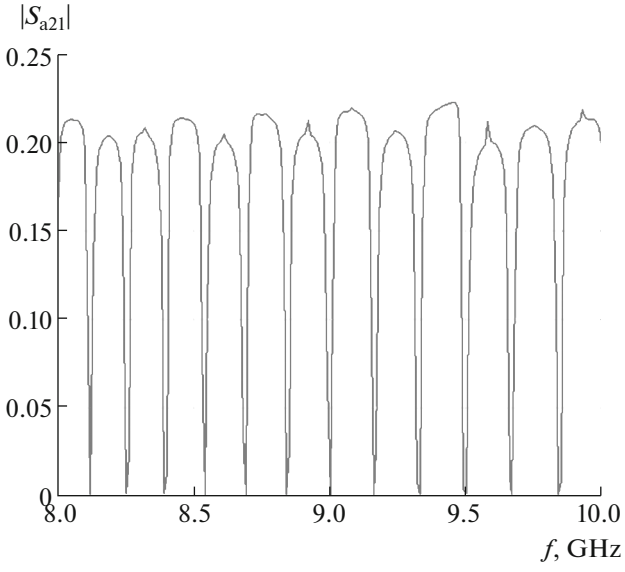

Fig. 6. Frequency dependence of the absolute value of the array transmission coefficient for $\varphi_n = 0$.

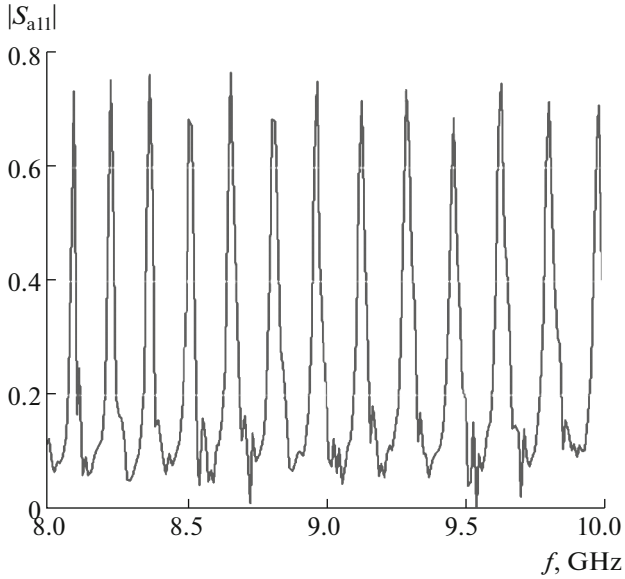

Fig. 7. Frequency dependence of the absolute value of the reflection coefficient at the array input for $\varphi_n \neq 0$.

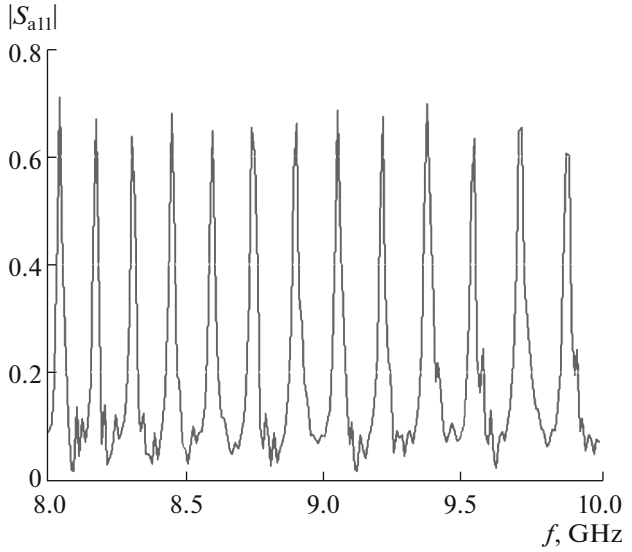

Fig. 8. Frequency dependence of the absolute value of the reflection coefficient at the array input for $\varphi_n \neq 0$ and different radiating and connecting waveguides.

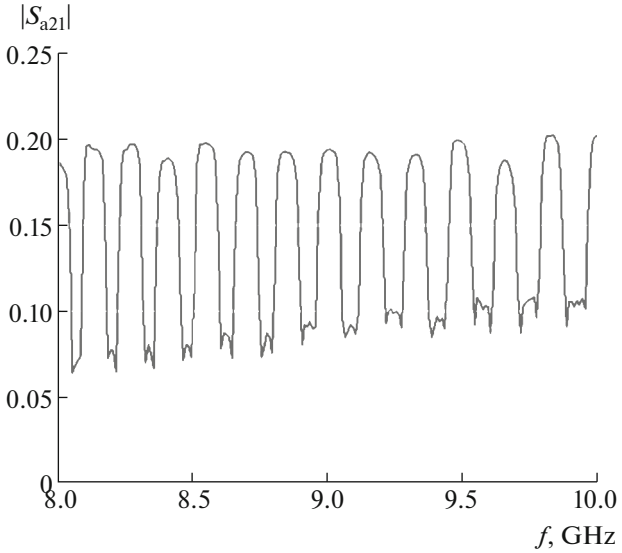

Fig. 9. Frequency dependence of the absolute value of the array transmission coefficient for $\varphi_n \neq 0$ and different radiating and connecting waveguides.

It is seen from formulas (14) that condition (2) holds true if these conditions are fulfilled. However, propagation constants and length of the waveguides are chosen such that summation of equiphase waves does not occur.

Frequency dependences of the absolute values of elements of the array scattering matrix, which are obtained after selection of parameters in accordance with equalities (8) and (14), are shown in Figs. 8 and 9. It is seen that maxima of the reflection coefficient are shifted substantially from the synthesis frequency. Here, we may speak of the existence of a frequency band in which the array is well matched. We should note that, similarly to Fig. 7, the positions of the maxima are not perfectly symmetric relative to the point $f = 9$ GHz.

The curve in Fig. 9 differs from the curve in Fig. 6 in that the zones in which the transmission coefficient is small become wider. They occupy bands substantially exceeding bands in which the array is mismatched. Thus, earlier, for $\varphi_n = 0$ and identical waveguides, we could relate lowering of the transmission coefficient with mismatch of the structure. However, we cannot make this now because there are frequency ranges in which both elements of the scattering matrix are small simultaneously.

In order to explain this fact, it is reasonable to consider the distribution of the wave amplitudes in the array. We will analyze amplitudes of the waves at the inputs of radiating waveguides. Let us assume that the wave traveling in the forward direction has amplitude U_n^+ and the wave traveling in the opposite direction has amplitude U_n^-. We introduce the concept of internal reflection coefficient R_n:

$$R_n = \left|\frac{U_n^-}{U_n^+}\right|. \tag{15}$$

The dependence of coefficient R_n on coordinate x_n is shown in Fig. 10. The curve was calculated at a frequency of 8.94 GHz at which absolute values of both elements of the array scattering matrix are close to 0.1,

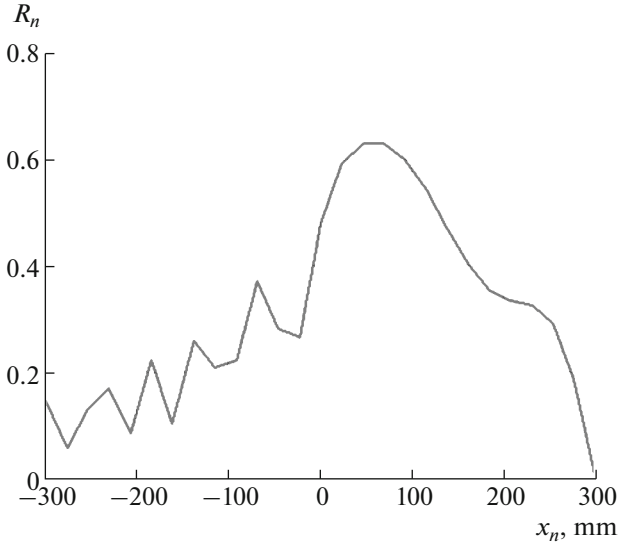

Fig. 10. Dependence of the absolute value of the internal reflection coefficient in the array on coordinate x at a frequency of 8.94 GHz.

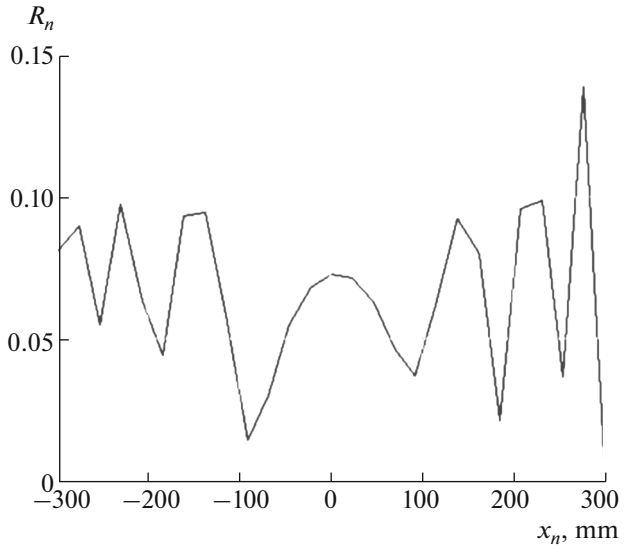

Fig. 11. Dependence of the absolute value of the internal reflection coefficient in the array on coordinate x at a frequency of 9 GHz.

i.e., they are rather small. It is seen that parameter R_n reaches a very substantial value inside the array. However, its value is substantially lower at the input; therefore, the array is well matched at its inputs. In this case, the field distribution inside the array is substantially different from a perfect distribution corresponding to the traveling-wave mode. Hence, widening of the frequency band in which the array has rather small transmission coefficient can be related to the appearance inside the array of a backward wave with a substantial amplitude, which is radiated into the free space but does not pass to input *1*. An additional radiation from the structure causes lowering of its transmission coefficient.

At frequencies for which the transmission coefficient is close to its maximum value, the internal reflection coefficient is small in all array channels. Its dependence on coordinate x_n is shown in Fig. 11. The figure was obtained at $f = 9$ GHz. It is of interest that the frequency band in which the transmission coefficient is close to the maximum value is symmetric relative to the array synthesis frequency.

The performed study allows us to deduce that the optimum traveling-wave mode exists in the array in frequency bands where parameter $|S_{a21}|$ is close to the maximum value S_{a21m}. This value is almost completely determined by number of radiators in the waveguide M, number of waveguides N, and conductance g:

$$S_{a21m} = \exp(-NM\delta), \quad \delta = g/2, \tag{16}$$

where δ is the wave attenuation at one radiator. Waves absorbed by the radiators form in the array aperture the distribution of sources exciting the free space. In the operating conditions close to the traveling-wave mode, it is close to a constant along the $0y$ axis and an exponent along the $0x$ axis.

3. MODEL OF RADIATION FROM THE ARRAY

In order to determine the radiation field, we should specify the type of the field source equivalent to an elementary radiator of the array as well as the source amplitudes. We have noted above that the equivalent circuit of the source in the form of a parallel conductance corresponds to a narrow longitudinal slot in the waveguide broad wall. It is generally agreed that its field is close to the field of a magnetic current oriented along the slot axis and is placed on the surface of the metal screen in which the slot is made. We will use below this model for calculation of the field in the focusing region. For simplicity, we will use magnetic current $I^{M}_{n,m}$ in the form of an elementary dipole:

$$I^{M}_{n,m} = A_{n,m}\delta(x - x_n)\delta(y - y_{n,m})\delta(z), \tag{17}$$

where $A_{n,m}$ is the amplitude of the magnetic dipole.

A more rigorous model of the radiator takes into account the finite length of the slot. However, for our analysis, it can be assumed to be zero, because radiation patterns of a short slot and an elementary dipole differ only slightly from each other.

The matrix model of the array allows us to determine amplitudes of magnetic currents to within an arbitrary factor C. We assume that amplitudes $A_{n,m}$ are proportional to the electric field in the radiation waveguide at the point where the array element is located. This field is proportional to the sum of amplitudes of the waves incident onto inputs *1* and *2* of the radiator, $U_{i1,2n,m}$, where subscripts *1* and *2* correspond to the number of the radiator input and subscripts n,m describe its position in the array. Wave amplitudes $U_{i1,2n,m}$ are assumed to be known, since they can be found in the framework of the matrix model. In this case, we can write:

$$A_{n,m} = C\left(U_{i1n,m} + U_{i2n,m}\right). \tag{18}$$

Factor C, which is common for all radiators, remains indefinite. The nonuniqueness in the writing of magnetic current amplitudes is caused by the fact that the matrix theory does not consider interaction between the array elements through the radiation field. On the one hand, using this model, we can find the power radiated in free space P_r from the power conservation law:

$$P_r = P_0\left(1 - |S_{a11}|^2 - |S_{a21}|^2\right), \tag{19}$$

where P_0 is the power of the wave incident onto the array input. On the other hand, we can calculate the radiation power directly through the integral of the Poynting vector of the field. Generally, these two

methods for calculation of the radiation power give different results; therefore, the energy balance in the array model is violated. In order to avoid this contradiction, we introduce factor C, which is chosen from the condition of equal values of the radiation power of magnetic currents and radiation power (19) in the matrix model.

The problem of determining factor C was solved in [24]. We give here the final result:

$$A^2 = -\frac{8\pi ik W P_0 \left(1 - |S_{a11}|^2 - |S_{a21}|^2\right)}{\sum_{n,m,p,q} \left(k^2 - \frac{\partial^2}{\partial y_m^2}\right)\left(J_{nm} J^*_{pq} \frac{\exp(-ikr_{nmpq})}{r_{nmpq}} - J_{pq} J^*_{nm} \frac{\exp(ikr_{nmpq})}{r_{nmpq}}\right)},$$
$$J_{n,m} = U_{i1n,m} + U_{i2n,m}, \quad r_{nmpq} = \sqrt{(x_n - x_p)^2 + (y_{n,m} - y_{p,q})^2}, \tag{20}$$

where the asterisk denotes the complex conjugate.

Vector magnetic potential A_y^M of the radiation field of magnetic currents is found with the help of the Green's function of free space [28]:

$$A_y^M = \frac{C}{2\pi} \sum_{n,m} \frac{\exp(-ik\rho_{n,m})}{\rho_{n,m}} J_{n,m},$$
$$\rho_{n,m} = \sqrt{(x - x_n)^2 + (y - y_{n,m})^2 + z^2}, \tag{21}$$

where x, y, z are the coordinates of the observation point. Transition from the vector potential to the electromagnetic field can be performed using the relationships from [28].

Directive gain D used in [24] is an important parameter describing the field focusing. It is defined as the ratio of the Poynting vector at the focusing point multiplied by the squared focal distance and the radiated power. As the focus moves toward infinity, the directive gain tends to a standard value for an antenna radiating in the far zone.

Along with the directive gain of the array, it is reasonable to introduce directive gain D_0 of a perfect aperture with continuous aperture distribution of sources. It is defined similarly to the directive gain of the array. The difference between parameter D_0 and the directive gain of the array lies in that a perfectly focused aperture has a nonuniform amplitude–phase distribution of sources $U_0(x, y)$. It is described by a function complex conjugate to the function setting the field of a spherical wave radiated from the focal point:

$$U_0(x, y) = \frac{\exp(ikR)}{R}, \quad R = \sqrt{x^2 + y^2 + z_f^2}. \tag{22}$$

Using two directive gains, we can find array aperture efficiency K:

$$K = \frac{D}{D_0}. \tag{23}$$

4. NUMERICAL ANALYSIS OF SCANNING

Let us consider several results obtained by means of numerical calculation of the array radiation field. As an example, we take an array designed on the basis of metal waveguides with a width of 22 containing longitudinal slots. The slots are excited with alternating phases. The structure has dimensions of 600 × 600. The period along the $0x$ axis is 23. The center frequency at which the array is synthesized is 9 GHz. The focal distance $z_f = 800$.

At the first stage, we consider motion of the focal spot in the case of scanning in plane XOZ. We have noted above that raster scanning does not occur under a continuous frequency variation. It occurs in several frequency bands (scanning zones). The focal spot moves along a curve close to plane XOZ in a zone containing the center frequency of 9 GHz. The scanning zones are characterized by number ν (see relationship (2)). In the case under study, the center scanning zone has number 25. Thus, at the first stage, we will analyze motion of the focal spot within the 25th zone.

Calculations were performed as follows. We selected certain spatial region in which we calculated the electric field generated by the array at some frequency f with some increments along coordinates $x, y,$ and z. Then we found field maximum E_m and its coordinates $X_m, Y_m,$ and Z_m. Let us denote the maximum value of the field at frequency f_0 by E_{m0}. For convenience, we introduce field E_n normalized by quantity E_{m0}.

The dependence of the absolute value of normalized component E_{ny} of the electric field on coordinate x is shown in Fig. 12. Curves *1–10* were obtained at frequencies spaced from 8.94 GHz with an increment of 0.01 GHz. Parameters of the array were given above. Curves *1–11* were obtained for $y = Y_m$ and $z = Z_m$. It is seen that the array efficiently concentrates field, which moves within ±400 as frequency varies in a range of 0.1 GHz. As frequency moves away from f_0, parameter E_m decreases. This change is especially

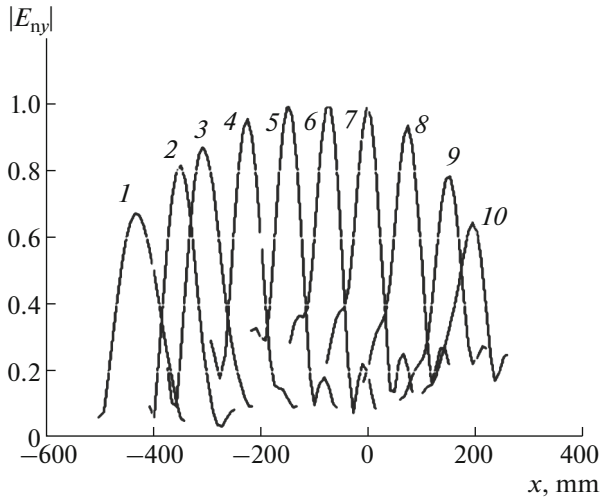

Fig. 12. Dependence of the absolute value of the normalized intensity of component E_{ny} of the electric field on coordinate x.

noticeable when the spot moves to the right, i.e., at relatively high frequencies.

Let us consider the shape of the focal spot in more detail. Dependences of the absolute value of the normalized intensity of the electric field on coordinates x, y, and z are shown in Figs. 13a–13c, respectively. The curves were obtained at center frequency f_0. Using Figs. 13a and 13b, we can determine the width of the focal spot at a level of – 3 dB, which is about 40 in both planes. Thus, we can deduce that the array concentrates field in a region slightly exceeding the wavelength. Naturally, as the focal spot moves away from the focal point, the field amplitude decreases and the spot broadens, which is seen from Fig. 12.

We should note asymmetry of the field distribution along both coordinate x and coordinate y. This asymmetry can be associated with an asymmetric relative to array center distribution of the field in plane XOY. The amplitude distribution of the field along longitudinal axis $0z$ is shown in Fig. 13c. It is seen that the field varies along this axis much more slowly than in the transverse plane. Such a behavior of the field is typical of all focused beams having large focusing depth in the longitudinal direction.

We should mention the presence of a noticeable background field existing at a substantial distance from the maximum point. The dependence of the absolute value of the normalized intensity of the electric field on coordinate x is shown in Fig. 14. The center part of the curve coincides with the curves in Fig. 13a. It is seen that, after an abrupt drop of the field in the center part of the focal spot, its rate of lowering decreases, which allows us to speak of the existence of a background field. It is possible that the appearance of this field is caused by the large spacing between

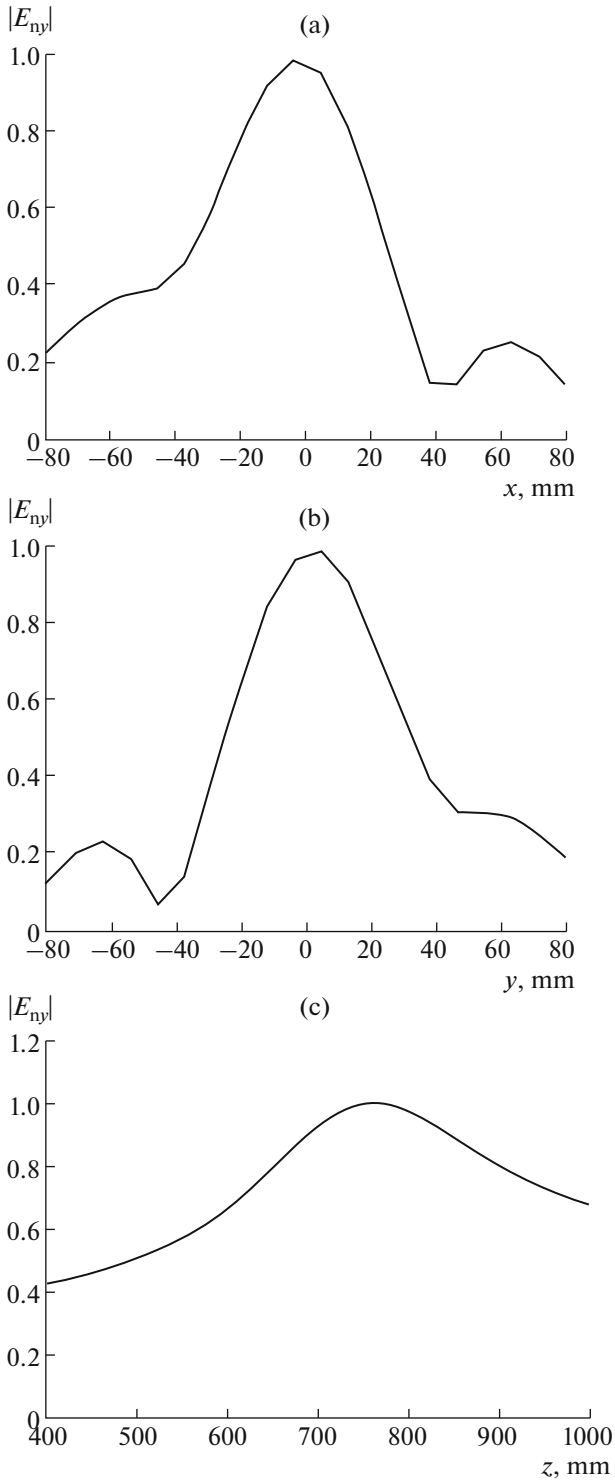

Fig. 13. Distribution of the absolute value of the normalized intensity of component E_{ny} of the electric field in the focal spot as a function of coordinate (a) x, (b) y, and (c) z.

radiators along the $0y$ axis in the lower part of the array (see Fig. 3). Evidently, an array with such a constant period would have not only the main radiation maximum but also grating maxima. In our case, the

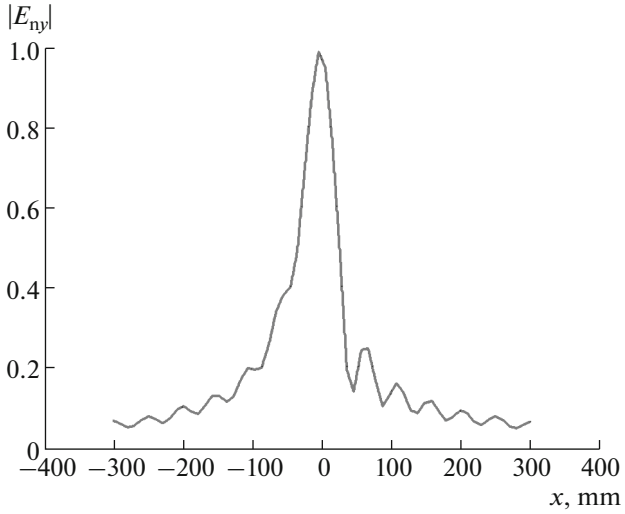

Fig. 14. Distribution of the absolute value of the normalized intensity of component E_{ny} of the electric field in the focal spot for a broad range of variation of coordinate x.

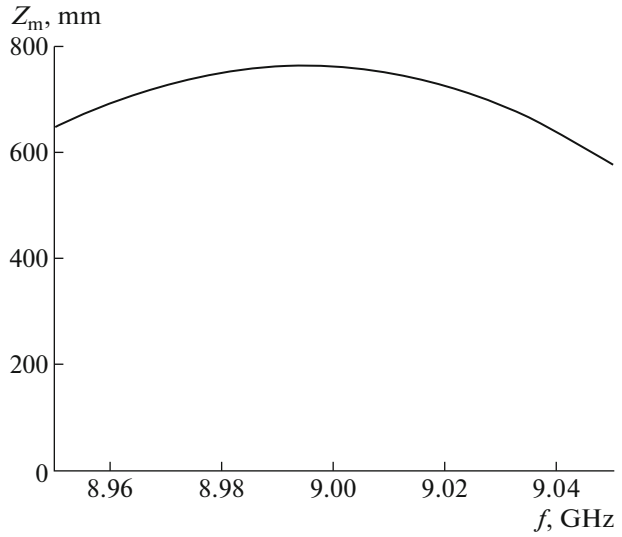

Fig. 15. Frequency dependence of coordinate Z_m of the field maximum along the $0z$ axis at $\nu = 25$.

array has a variable period and explicit formation of grating maxima does not occur. However, the difference from a system of point radiators may appear in the form of the aforementioned background field.

The frequency dependence of coordinate Z_m is shown in Fig. 15 and the motion trajectory of the field maximum in plane XOY is presented in Fig. 16. We should note that, even at a frequency of 9 GHz, the position of the field maximum does not coincide with the conventional focal point used in the synthesis of this structure. Coordinate Z_m of the maximum point is 40 mm less than focal distance z_f.

Further study of this array consists in the analysis of its behavior in other scanning zones. Calculations were performed in frequency bands of ±0.05 GHz located around frequencies f_ν. Motion trajectories of the field maximum in planes XOY and XOZ are shown in Figs. 17a and 17b. Curves *1*–*7* were obtained for $\nu = 18, 21, 24, 25, 26, 29,$ and 32. The array parameters were given above.

The rate of motion of the focal spot along the $0x$ axis at high frequencies is larger than at low frequencies. For this reason, the length of the spot trajectory in plane XOY decreases in zones with larger numbers at a constant frequency range. We can note that, at relatively high frequencies, the spot moves along the $0y$ axis also more slowly than at low frequencies. For this reason, the upper trajectory is shifted by 130 mm relative to the zero level and the lower trajectory is shifted by 160 mm. Note that the frequency interval separating zones with $\nu = 18$ and 32 is approximately 2 GHz.

The spot motion trajectory in plane XOZ resembles an arc centered at the point $x = z = 0$. In the case of strong deviation from the main scanning zone with $\nu = 25$, we observe distortion of trajectories, which become substantially asymmetric.

Figure 18 presents the dependence of the maximum of the normalized field intensity in the focal spot on parameter δf:

$$\delta f = f - f_\nu. \tag{24}$$

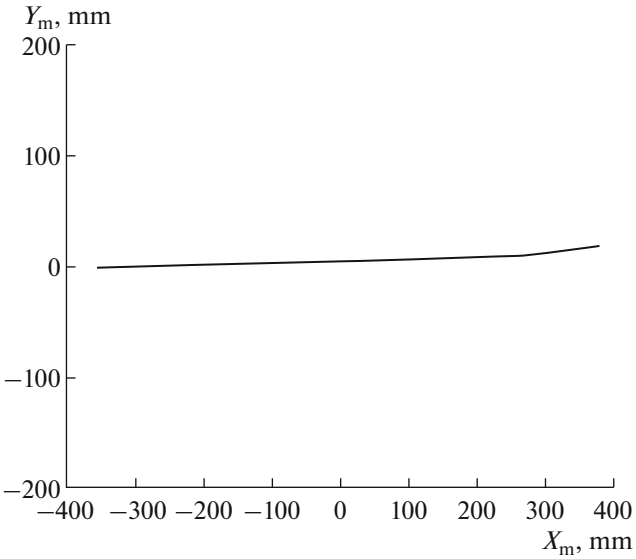

Fig. 16. Dependence of coordinate Y_m of the field maximum along the $0y$ axis on coordinate X_m of the field maximum along the $0x$ axis at $\nu = 25$.

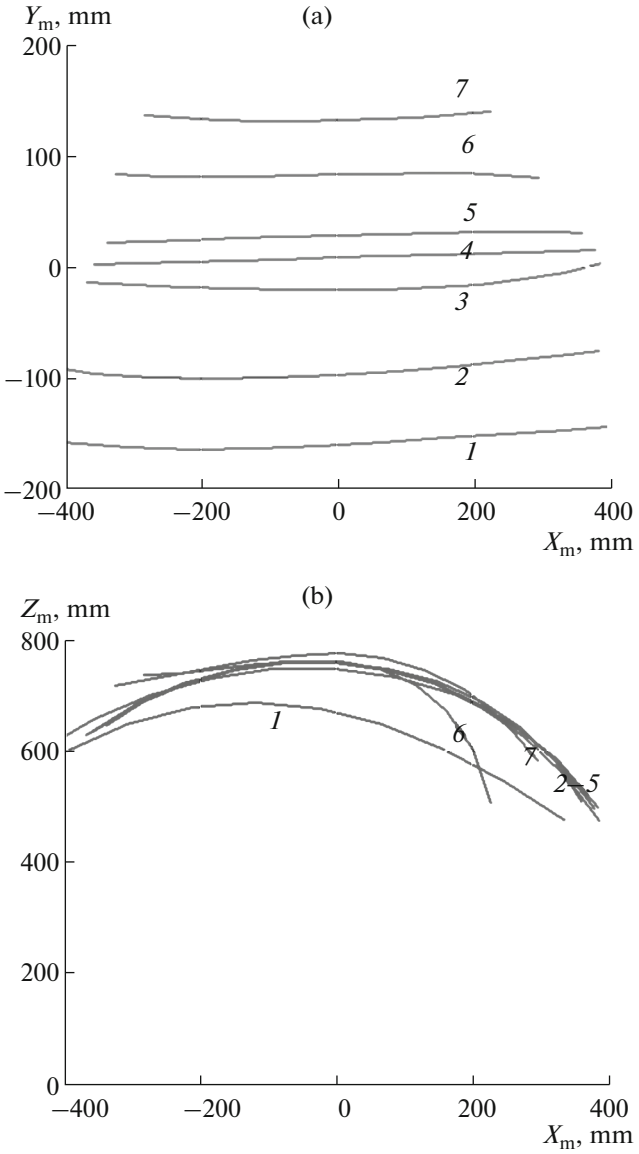

Fig. 17. Dependences of the (a) coordinate Y_m of the field maximum along the $0z$ axis and (b) coordinate Z_m of the field maximum along the $0z$ axis on coordinate X_m of the field maximum along the $0x$ axis for $\nu = 18, 21, 24, 25, 26, 29$, and 32 (curves *1*–*7*, respectively).

Curves *1*–*7* were obtained for ν = 18, 21, 24, 25, 26, 29, and 32. The frequency range chosen for plotting the curves is chosen such that the field intensity at its edges lowers by approximately 3 dB relative to the maximum value. It can be readily noticed that this range is asymmetric relative to frequencies f_ν, it is shifted toward the region of low frequencies. The cause of this shift is associated with rapid lowering of the field intensity with increasing frequency.

Calculations have shown that the increase in the field value within the scanning zone in the region of

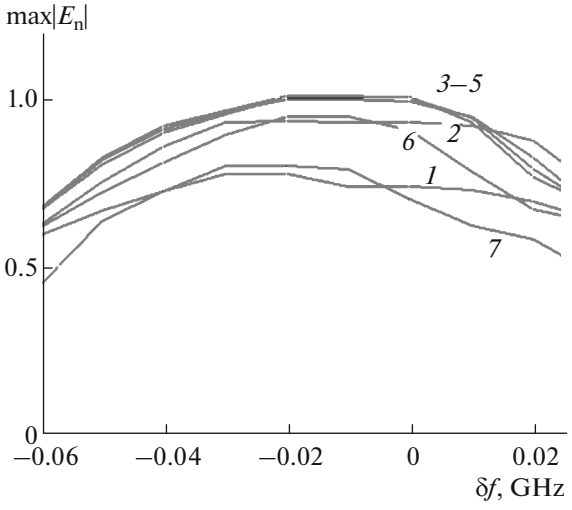

Fig. 18. Frequency dependence of the maximum field value.

high frequencies is caused by radiation of a certain portion of energy in directions distant from the focusing point, rather than changes in the amplitude–phase distribution in the antenna aperture. This effect can be related to the existence of regions with large periods along both the $0x$ and the $0y$ axes in the array. The structure under study is aperiodic and speaking of its periods is not quite correct. However, the spacing between radiators within the aperture varies rather slowly; therefore, we can consider this array locally periodic if we consider the spacing between its elements in a given spatial region as a period. Moreover, it is strictly periodic along the $0x$ axis.

In the considered example, the period along the $0x$ axis is 23 whereas wavelength λ in the vicinity of the center frequency is approximately 33. At frequency f_0, parts of the array with different positions along the $0x$ axis radiate into the focusing point at angles not exceeding critical angle θ_c corresponding to the angle of the subsidiary diffraction maximum:

$$\sin\theta_c = \frac{\lambda}{P_x} - 1. \qquad (25)$$

However, as the spot is deviated, it is seen from some array parts at an angle exceeding the critical angle. In this case, a substantial portion of energy from this part is radiated not in the field focusing direction are creates the aforementioned parasitic background.

If the spot is shifted to the right (which occurs ate relatively high frequencies), such parts are located in the left region of the array. On the contrary, if the spot is shifted to the left, the array operates in a nonoptimal mode in the right region. It should be taken into account that the left and right regions of the array are not identical, because the amplitude distribution of sources along the $0x$ axis has an asymmetric exponen-

tial form. Since we consider excitation of the structure at the left (input *1*), the maximum of the amplitude distribution is located at the left edge of the array. For this reason, incorrect operation of the left part of the array, which takes place in the high-frequency range, results in a substantially larger lowering of the field value in the focusing region than in the case of frequency shift toward the region of low frequencies.

The presented interpretation of the obtained effect allows us to explain its stronger manifestation in zones with large numbers (curve *7* in Fig. 18) than in zones with small numbers (curve *1* in Fig. 18). These zones have widely spaced frequencies; therefore, angle θ_c in the zone with $\nu = 18$ is substantially larger than in the zone with $\nu = 32$ and the shift of the spot in this zone may be large.

The frequency dependence of the aperture efficiency of the focused array with parameters given above is shown in Fig. 19. Curves *1*–*3* were obtained for $P_x = 18, 20.5,$ and 23. The array was synthesized at a frequency of 9 GHz for operation in the main scanning zone with $\nu = 25$. It is seen that, for relatively small periods, the aperture efficiency of this array is close to –3 dB. An increase in the period along the $0x$ axis causes additional lowering of the aperture efficiency.

We can suppose that the array has relatively low aperture efficiency because of the existence of the aforementioned regions with large local periods. The array has the largest period along the $0y$ axis in the region of negative y. The appearance of regions with large period is related to the field focusing above the structure center. For such a position of the focus, elements located in the region $y < 0$ radiate into the forward half-space relatively to the direction of propagation of the waves in radiating waveguides and elements located in the region $y > 0$ radiate in the backward direction. Radiation in the forward direction is possible only in arrays with large periods. It is possible to avoid the appearance of such regions by shifting the focusing point toward negative values of y. However, this is undesirable for many practical applications. The interelement spacing can be reduced with the help of waveguides with slow waves. Such a change in the design has negative consequences caused by the fact that, as a rule, the attenuation in such waveguides is substantially larger than the attenuation in hollow metal structures. Here, because of a large total length of the waveguide circuit forming the array, the problem of the loss caused by the attenuation in this circuit is very important.

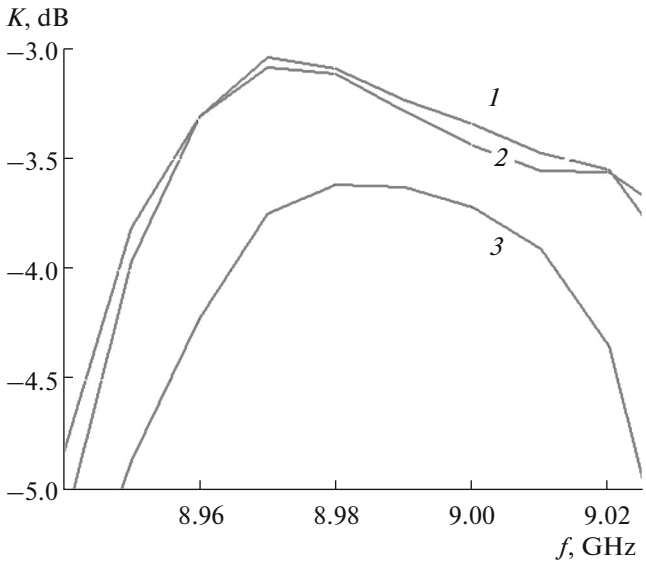

Fig. 19. Frequency dependence of the array aperture efficiency.

CONCLUSIONS

The results presented in this paper do not provide complete solution to the problem of detailed analysis of an array with raster scanning. These results should be considered as its first stage at which we have estimated the potentialities of the structure in the first approximation. However, even first results allow us to outline directions of further investigations and formulate topical problems. Let us enumerate some of these problems:

(i) Building of an electromagnetic model of the array and the analysis of its characteristics with consideration for the effects of the structural elements.

(ii) Analysis of arrays based on different types of transmission lines, including waveguides with slow waves.

(iii) Analysis of 180° bends of transmission lines aimed at improvement of their matching in a wide frequency band.

(iv) Analysis of arrays with consideration for the effect of the thermal loss.

The results presented above allow us to deduce that practical application of focused arrays with raster scanning may have prospects for the design of radio lenses. They are of interest due to their simplest design ensuring low cost of the system. However, the simplest design causes certain problems. Some of these problems were described above. Among such problems is rapid increase in the array reflection coefficient when the focal spot is located in plane XOZ. The presented data have shown that these problems can be rather efficiently solved; therefore, the appearance of such problems cannot change the general positive conclusion about prospects of the analyzed structures.

REFERENCES

1. D. M. Sheen, D. L. McMakin, and T. E. Hall, Proc. SPIE **4032**, 52 (2000).

2. D. A. Robertson, S. L. Cassidy, B. Jones, and A. Clark, Proc. SPIE **9078**, 907805 (2014).
3. S. S. Ahmed, A. Schiessl, and L.-P. Schmidt, IEEE Trans. Microwave Theory Tech. **59**, 3567 (2011).
4. S. E. Bankov, V. A. Kaloshin, and E. V. Frolova, in *Radiolocation and Radio Communication (Proc. XVI Int. Conf., Firsanovka, Moscow oblast, Nov. 11–16, 2008)* (MEI, Moscow, 2008), p. 390.
5. V. A. Kaloshin and E. V. Frolova, in *Radiolocation and Radio Communication (Proc. IV All-Russia Sci.–Eng. Conf., Moscow, Nov. 29 – Dec. 3, 2010* (IRE RAN, Moscow, 2010), p. 432.
6. N. J. Bowring, M. J. Southgate, and D. A. Andrews, et al., Proc. SPIE **8714**, 87140C (2013).
7. E. Heinz, T. May, and D. Born, et al., Opt. Eng. **50**, 113204 (2011).
8. E. N. Grossman, J. Gordon, D. Novotny, and R. Chamberlin, Proc. SPIE **9078**, 907809 (2014).
9. N. E. Alexander, B. Alderman, and F. Allona, et al., Proc. SPIE **9078**, 907802 (2014).
10. E. Gandini, N. Llombart, and A. Neto, in *Proc. 2014 IEEE Antennas and Propagation Soc. Int. Symp. (APSURSI), Memphis, Jul. 6–11, 2014* (IEEE, New York, 2014), p. 1471.
11. E. Schreiber, M. Peichl, M. Jirousek, and H. Suess, Proc. SPIE **8715**, 87150J (2013).
12. E. Gandini, M. Ettorre, M. Casaletti, et al., IEEE Antennas Wireless Propag. Lett. **11**, 1572 (2012).
13. S. E. Bankov, G. G. Grachev, M. D. Duplenkova, and E. V. Frolova, J. Commun. Technol. Electron. **59**, 504 (2014).
14. I. Ohtera, IEEE Trans. Antennas Propag. **38**, 121 (1990).
15. I. Ohtera, IEEE Trans. Antennas Propag. **47**, 1470 (1999).
16. J. L. Gómez-Tornero, F. Quesada-Pereira, A. Alvarez-Melcón, et al., IEEE Trans. Antennas Propag. **59**, 407 (2011).
17. A. J. Martínez-Ros, J. L. Gómez-Tornero, F. J. Clemente-Fernández, and J. Monzó-Cabrera, IEEE Trans. Antennas Propag. **61**, 2981 (2013).
18. T. Okuyama, Y. Monnai, and H. Shinoda, IEEE Trans. Antennas Propag. **61**, 1284 (2013).
19. S. Clauzier, S. Avrillon, L. Le Coq, et al., IET Microwaves, Antennas & Propag. **9**, 634 (2014).
20. M. L. Chen, S. Gupta, Z. L. Ma, and L. J. Jiang, *in Proc. 2014 IEEE Antennas and Propagation Soc. Int. Symp. (APSURSI), Memphis, July 6–11, 2014* (IEEE, New York, 2014), p. 1047.
21. J. L. Gómez-Tornero, A. J. Martinez-Ros, D. N. Blanco, and E. Rajo-Iglesias, in *Proc. 6th Eur. Conf. on Antennas and Propagation (EuCAP), Prague, Mar. 26–30, 2012* (IEEE, New York, 2012), p. 234.
22. D. Blanco, J. L. Gómez-Tornero, E. Rajo-Iglesias, and N. Llombart, IEEE Antennas Wireless Propag. Lett. **13**, 583 (2014).
23. M. Ettorre, M. Casaletti, G. Valerio, et al., IEEE Trans. Antennas Propag. **62**, 1991 (2014).
24. S. E. Bankov, V. A. Kaloshin, and E. V. Frolova, J. Commun. Technol. Electron. **61**, 587 (2016).
25. R. Hansen, *Microwave Scanning Antennas* (Academic, 1964; Sovetskoe Radio, Moscow, 1966), Vol. 1.
26. S. E. Bankov, *Arrays with Series Feeding* (Fizmatlit, Moscow, 2013) [in Russian].
27. D. M. Sazonov, *Microwave Circuits and Antennas* (Vysshaya Shkola, Moscow, 1988; Mir, Moscow, 1990).
28. G. T. Markov and A. F. Chaplin, *Excitation of Electromagnetic Waves* (Radio i Svyaz', Moscow, 1983) [in Russian].

Translated by A. Kondrat'ev